Geophysical Research Letters

RESEARCH LETTER
10.1029/2025GL115080

# Coupling Between Methylmercury and Carbon-Gases Across Boreal Rivers of Québec, Canada

A. Campeau[1,2,3,4], M. Amyot[4,5], P. del Giorgio[4,6], C. Fink-Mercier[5], M. Wauthy[5], D. E. Ponton[4,5], and J.-F. Lapierre[4,5]

[1]Department of Geography, University of Montréal, Montréal, QC, Canada, [2]Department of forest ecology and management, Swedish university of agricultural sciences, Umeå, Sweden, [3]Department of Geography, McGill University, Montréal, QC, Canada, [4]Groupe de Recherche Interuniversitaire en Limnologie (GRIL), Montréal, QC, Canada, [5]Department of Biological Sciences, University of Montréal, Montréal, QC, Canada, [6]Department of Biological Sciences, University of Québec in Montréal (UQÀM), Montréal, QC, Canada

**Key Points:**

- Multi-regional synthesis of 537 boreal river water samples reveals a large-scale coupling between methylmercury and carbon gases
- Methylmercury-methane correlations strengthen when accounting for oxidation, revealing coupling beyond localized anoxic processes
- Regional Hg-C coupling shifts from terrestrial co-loading in cold, wetland-rich areas to in-stream processes in warmer impounded rivers

**Supporting Information:**

Supporting Information may be found in the online version of this article.

**Correspondence to:**

A. Campeau,
audrey.campeau@umontreal.ca

**Citation:**

Campeau, A., Amyot, M., del Giorgio, P., Fink-Mercier, C., Wauthy, M., Ponton, D. E., & Lapierre, J.-F. (2025). Coupling between methylmercury and carbon-gases across boreal rivers of Québec, Canada. *Geophysical Research Letters*, *52*, e2025GL115080. https://doi.org/10.1029/2025GL115080

Received 28 JAN 2025
Accepted 23 MAY 2025



**Abstract** We examine correlations between mercury (Hg) and carbon (C) concentrations and speciation by synthesizing 526 river water samples across three distinct regions in Québec, Canada (48° to 55°N and 62° to 80°W). Positive correlations between methylmercury (MeHg) per unit Hg and C-gases per unit dissolved organic carbon suggest Hg-C co-transformation within rivers. Correlations between MeHg and methane ($CH_4$) concentrations strengthen when adjusted for oxidation, revealing an association that goes beyond the established link between fermentation and Hg methylation in anoxic environments. These correlations persist but are manifested differently across regions. Colder, wetland-dominated regions indicated stronger terrestrial co-loading, while warmer and more recently impounded systems exhibited more co-transformation. These findings emphasize the interconnected biogeochemical cycles of Hg-C in northern rivers and highlight the importance of landscape characteristics influencing their coupling.

**Plain Language Summary** The concentrations of organic carbon and mercury are typically strongly related in aquatic ecosystems. The transformation of organic carbon and mercury, although occurring through different processes, can lead to various by-products, including carbon dioxide and methane, two major greenhouse gases, and methylmercury, a neurotoxin. There is growing evidence of a coupling in the occurrence of carbon and mercury by-products within rivers, but this link has not been explored across large spatial scales. Here we show multiple evidence of a broad correlation between methylmercury concentrations and greenhouse gases across >100 sites of boreal rivers across Québec, Canada. This suggests that the carbon and mercury cycles are further linked through the co-production of their respective by-products in boreal rivers. Resolving the geographic variability in this coupling will be important to better understand and predict environmental relevance.

## 1. Introduction

Mercury is a potentially hazardous neurotoxin whose biogeochemical cycle has been greatly altered by human activities (Driscoll et al., 2013; Selin, 2009). Through long-range atmospheric transport, anthropogenic Hg is deposited in pristine ecosystems far from its emission point (Braune et al., 2015; Driscoll et al., 2013) where it binds to organic matter (OM) in terrestrial and aquatic environments (Bishop et al., 2020; Haitzer et al., 2002; Skyllberg et al., 2006). Surface runoff loads this Hg-OM complex into rivers and streams, where it can be transported into downstream water bodies (Emmerton et al., 2022; Hebert, 2019; Schartup et al., 2015). Both Hg and dissolved organic matter (DOM) can undergo transformation in aquatic systems through separate but potentially linked processes (Lawruk-Desjardins et al., 2024). Transformation of Hg and dissolved organic carbon (DOC) can give rise to multiple by-products of environmental relevance, including methylmercury (MeHg), the most bioaccumulative form of Hg (Ullrich et al., 2001), and carbon dioxide ($CO_2$) or methane ($CH_4$), two important greenhouse gases (Raymond et al., 2013; Rocher-Ros et al., 2023).

While Hg and C coupling through their co-loading from terrestrial sources and co-transportation in rivers is well-established, their possible co-transformation at the landscape scale is less clear, despite a clear metabolic link between methylation and fermentation in anoxic environments (Pak & Bartha, 1998; Zhu et al., 2018). Recent studies at individual catchment scale have identified a correlation between the methylated proportion of the Hg pool and the presence of both $CO_2$ and $CH_4$ (Amyot et al., 2024; Bonville et al., 2020; MacMillan et al., 2015).

10.1029/2025GL115080

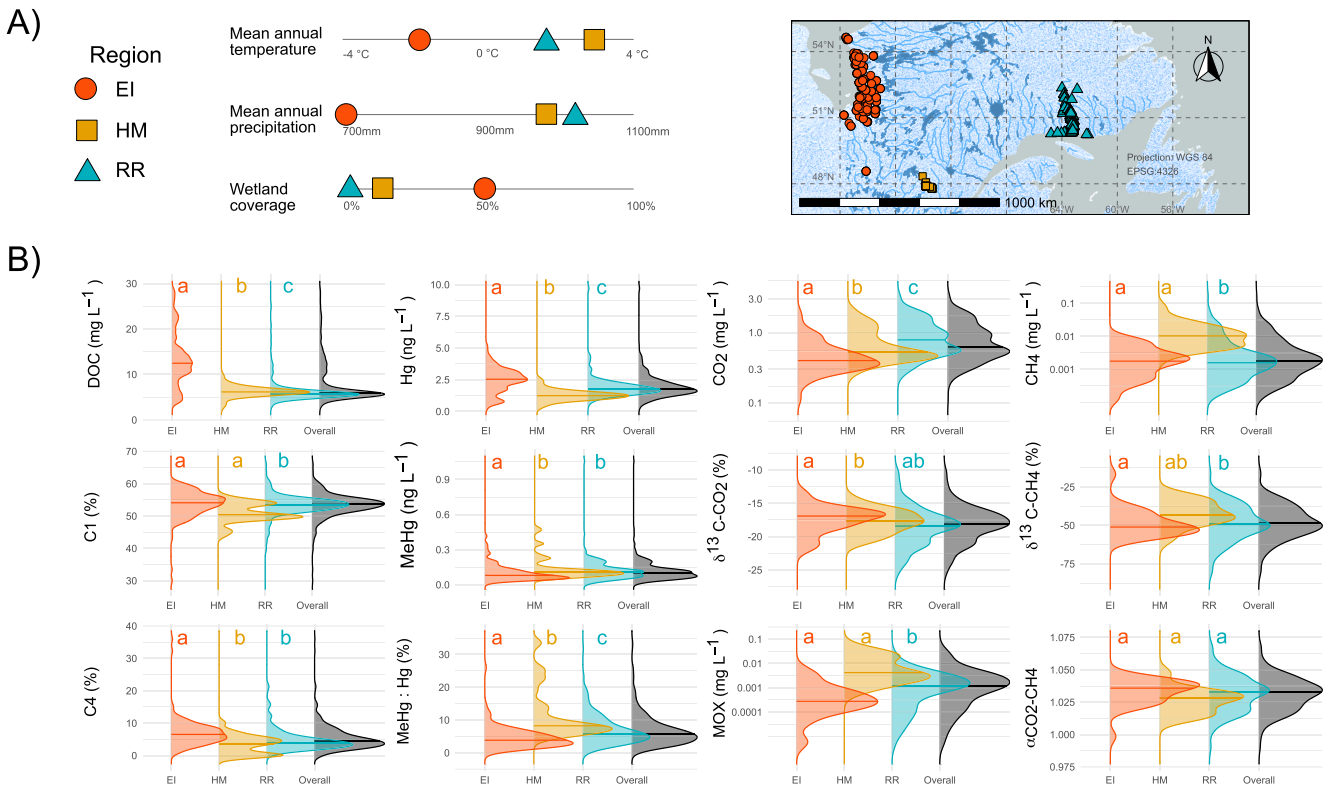


**Figure 1.** (a) Map of the river water sampling locations, in three different regions (orange (EI) Eeyou Istchee, yellow (HM) Haute-Mauricie, blue (RR) Romaine River) together with a summary table of their key landscape and climatic properties. (b) Ridge plots summarizing river water chemistry variables for each region, with the same colour code. Letters on the top x-axis denote the results from the Dunn's test and indicate statistically significant differences between the medians of each region. An interactive version of the map is available on this GitHub page.

Whether this coupling persists across multiple river systems and how it might shift across diverse landscape types is unclear.

The goal of this study is to examine the coupling between Hg and C cycling in river systems across large geographical scales. For this, we assembled 526 river water samples across 113 separate locations. These rivers include both harnessed and free-flowing river systems, spanning from small tributaries (~10 m width) to larger river channels (>100 m width), and scattered across three different regions of Québec, Canada (48° to 55°N and 62° to 80°W). We combined multiple independent metrics (i.e., concentration, speciation, DOC fluorescence and stable C isotope ratios) to examine the coupling between the Hg and C cycle. We specifically assess (a) whether there is a coupling between Hg and C by-products across all rivers, (b) if this coupling could arise simply from the co-occurrence of methanogenesis and mercury methylation in anoxic environments and (c) how this coupling is manifested across different landscape types. Our synthesis reveals previously unrecognized large-scale coupling in the Hg-C transformation in rivers, establishing a foundation for future investigation of the landscape controls over their interconnected biogeochemical cycles.

## 2. Materials and Methods

### 2.1. Regional Landscape Characteristics

This study combines data that were previously collected and published for rivers in three distinct regions of Québec: the Eeyou Istchee (EI) region of Eastern James Bay ($n$ = 122) (Fink-Mercier, Lapierre, et al., 2022), La Romaine River (RR) in the maritime boreal region of la Côte-Nord ($n$ = 355) (Bonville et al., 2020), and St. Maurice River in the central boreal region of Haute-Mauricie (HM) ($n$ = 49) (Ponton et al., 2021) (Figure 1a). The rivers sampled in the EI region comprise 18 individual large river systems that are both dammed and free flowing. These rivers were often sampled at three different locations (upstream, halfway and near the mouth) and visited on five separate occasions, from March to September, in 2018–2019. The sampling design of the HM and RR

focused on a single large river catchment. HM was visited three times around the end of summer in 2016-2017-2018. The samples from HM were collected along a river continuum, which contains 4 run-of-river dams, two of which were built as early as 2008 (Ponton et al., 2021). The samples from RR include a sequence of four reservoirs along the main stem, built between 2009 and 2022 (Bonville et al., 2020), together with several tributaries that are free-flowing and of variable sizes. The RR region was visited on five separate occasions, mostly during summer between 2017 and 2019. More details on the sampling of these regions have been published for EI (Fink-Mercier, Lapierre, et al., 2022), RR (Bonville et al., 2020) and HM (Ponton et al., 2021) areas.

These three regions are separated by a distance of up to 1,000 km, and therefore cover wide climatic and geographic gradients and differ substantially in landscape features. Seasonality is comparable across all three regions with annual temperatures varying from a maximum in July to a minimum in January, and evenly distributed precipitation across the year. Snow precipitation represents 20%–40% of the total annual precipitation and occurs mostly between November and April. The mean annual temperature is highest in HM (3.3°C La Tuque), followed by RR (1.7°C Natashquan), and EI (−2.2°C La Grande River) (Figure 1a, Climate Normals 1991–2020, Environment Canada). The mean annual precipitation is highest in RR (1,040 mm), followed by HM (9,935 mm), and EI (702 mm) (Figure 1a). The forest type for all three regions is boreal, although RR is found in the spruce-moss forest domain, HM in the balsam fir-white and yellow birch domain and EI in the spruce-moss and lichen domain. The fraction of land cover occupied by wetlands is far superior in EI (20%–75%) compared with HM (5%–20%) and RR (1%–5%) (Tarnocai et al., 2011) (Figure 1a). All three regions are found within the Canadian Shield, a strongly weathering-resistant bedrock. The atmospheric Hg deposition rate is relatively similar between the three regions (Nasr & Arp, 2017).

### 2.2. River Water Collection Procedure

Water samples were generally collected 0.5 m below the surface using a peristaltic pump with a 0.45 µm polycarbonate in-line filter (GWV high-capacity groundwater sampling capsules) connected to a Teflon tube. All pumping and filtering materials were acid-washed (HCl 10%, volume/volume (v/v)) and rinsed (Milli-Q ultrapure water) between sampling sites then rinsed with in situ water before sample collection.

Water samples for dissolved mercury (Hg) analysis were stored in acid-washed borosilicate amber glass bottles (washed with 45% $HNO_3$, and 5% HCl, v/v). Samples were acidified with concentrated HCl to reach a final concentration of 0.4% (500 µL in 125 mL). A total of 15 duplicates of field blanks were performed across the different field campaigns at EI ($n = 5$), HM ($n = 5$) and RR ($n = 5$). The mean Hg concentration of blanks in each geographical region was well below ambient concentrations and close to detection limits (Fink-Mercier, Giorgio, et al., 2022).

Water samples for DOC concentration and fluorescence analysis were collected with a peristaltic pump, filtered into a 0.45 µm filter and stored in amber borosilicate bottles, priorly washed in 10% HCl and burned at 450°C for 6–12 hr, more details in Fink-Mercier, Giorgio, et al. (2022). All river water samples were stored at 4°C in the dark.

### 2.3. Chemical and Optical Analyses

The concentration of Hg was obtained using the Tekran 2,600 (Tekran® Instruments Corporation, Toronto, ON, Canada) cold vapor atomic fluorescence spectrometer (CVAFS) with a detection limit of 0.05 ng $L^{-1}$ of Hg and following the 1,631 method of the United States Environment Protection Agency (EPA) (U.S. Environmental Protection Agency, 2002). Dissolved methylmercury (MeHg) concentration was measured using the Tekran 2,700 instrument CVAFS with a detection limit of 0.01 ng $L^{-1}$ and following the 1,630 method of the EPA (U.S. Environmental Protection Agency, 2001). All Hg concentration measurements were performed in duplicates of filtered samples for RR and EI data sets and in triplicate for HM. Blanks and standards were analyzed alongside samples to monitor the instrument's performance and stability. The accuracy of the method was independently confirmed by Proficiency Testing Canada.

The concentration of DOC was measured on a TIC-TOC Analyzer using wet persulfate oxidation (Aurora, College Station, TX, USA). DOM fluorescence and absorbance were measured using a UV-1,800 (Shimadzu, Kyoto, Japan) or an Ultrospec 3,100 Pro (Biochrom, Cambridge, UK) spectrophotometer, depending on sample origin, whereas 3-D fluorescence scans were run with a Cary Eclipse fluorescence spectrophotometer (Agilent

Technologies, Santa Clara, CA, USA). A parallel factor analysis was performed as described in Bonville et al. (2020). The model identified four fluorescence components (Figure S2 in Supporting Information S1), of which two shared fluorescence characteristics with humic and fulvic materials from terrestrial sources (C1–C3). The last component (C4) presented spectra similar to amino acids or proteins typical of algal production or recent production from surrounding terrestrial environments (Kothawala et al., 2014; Lapierre & Giorgio, 2014) (more details in Table S1 in Supporting Information S1).

The partial pressure of $CO_2$ and $CH_4$ in river water ($pCO_2$, $pCH_4$ in µatm) was obtained using the headspace equilibrium technique with zero gas, based on the methods and equations described in Campeau et al. (2014). The stable isotope ratio ($\delta^{13}C$) of $CO_2$ and $CH_4$ was measured on headspace samples on a cavity ringdown spectrometer (CRDS, Picarro 2201-i). The original concentration and $\delta^{13}C$ value of $CO_2$ and $CH_4$ in the water were then calculated as a function of these headspace values, headspace ratios, temperature, pressure, and the isotopic fractionation across the liquid-gas interface. The original surface water $pCO_2$ and $pCH_4$ were then calculated according to the headspace ratio, assuming a constant ambient air of 1.77 µatm for $pCH_4$ and field-measured $pCO_2$ from the EGM-4, and in EI, the ultraportable GHG analyzer (Los Gatos Research). Gas concentrations were later converted to mg C $L^{-1}$ following Henry's constant based on ambient pressure and temperature, as described in (Campeau et al., 2014).

### 2.4. Methane Oxidation Calculations

We reconstructed the potential total riverine $CH_4$ mass based on the measured ambient $CH_4$ mass together with the estimated mass of oxidized $CH_4$ (MOX). The MOX was first estimated by deriving the fraction of oxidized $CH_4$ (FOX) using the following equation adapted from Thottathil et al. (2018):

$$\mathrm{FOX} = \left(\delta^{13}\mathrm{C–CH}_{4\mathrm{sample}} - \delta^{13}\mathrm{C–CH}_{4\mathrm{source}}\right) / \left((\alpha_{\mathrm{app}} - 1) \times 1000\right) \quad (1)$$

where the $\delta^{13}C–CH_{4sample}$ is the value observed in the sample and the $\delta^{13}C–CH_{4source}$ is the theoretical value of the $CH_4$ source. The $\alpha_{app}$ is the apparent fractionation factor between $\delta^{13}C$-$CO_2$ and $\delta^{13}C$-$CH_4$ in each sample. Larger deviations between the $\delta^{13}C–CH_{4sample}$ and the $\delta^{13}C–CH_{4source}$ and a low $\alpha_{app}$ (i.e., more similar $\delta^{13}C$-$CO_2$ and $\delta^{13}C$-$CH_4$ values) yield a higher potential FOX.

The $\delta^{13}C–CH_{4source}$ was determined using the Miller-Tans plot and corresponded to −51.7% for all regions combined (Figure S3A in Supporting Information S1 (Campeau et al., 2017)). This is a relatively enriched $\delta^{13}C–CH_{4source}$ value and results in more conservative estimates of FOX. Most of our observations indicated a dominance of $CH_4$ oxidation ($n$ = 133, ε above −40%), with methanogenesis dominated by the acetolactic pathway ($n$ = 39, ε between −55 and −40%) (Figure S3B in Supporting Information S1 (Whiticar, 1999)). There were a few observations where methanogenesis was apparently dominated by the hydrogenotrophic pathway ($n$ = 4 for ε below −55%, exclusively in RR), which were excluded from the Miller-Tans analysis (outlier Figure S3 in Supporting Information S1).

The MOX was subsequently derived as the product of FOX and the ambient [$CH_4$] in the sample, expressed in mg C $L^{-1}$. Therefore, the MOX + [$CH_4$], both expressed in mg C $L^{-1}$, represents an estimate of the total $CH_4$ concentration, in the absence of $CH_4$ oxidation. When the estimated FOX was negative, we considered no $CH_4$ oxidation occurred in those samples (i.e., MOX is equal to zero). Negative FOX estimates occur when the $\delta^{13}C–CH_{4sample}$ is more negative than the $\delta^{13}C–CH_{4source}$. This was the case for 35% of our total observations, with a lower occurrence in the waters of HM region (12%) and the highest occurrence in the rivers of EI (50%), which reflected the overall low $CH_4$ concentration in the samples of EI.

The estimates of FOX and MOX were not used for budget purposes but rather to derive general patterns in $CH_4$ oxidation and possible correlations with riverine Hg and MeHg concentrations. We consider that this estimate of MOX is closer to ambient rates of $CH_4$ production, which we hypothesize should be a better proxy of [MeHg] than ambient $CH_4$ concentration because of the low volatility of MeHg compared with $CH_4$ and the high $CH_4$ oxidation potential of these rivers (Thottathil et al., 2018).

### 2.5. Statistical Analysis

We conducted non-parametric pairwise comparisons using Dunn's test for medians and Levene's test for variances. Spearman *rho* correlation on ranked values was used to identify statistically significant correlations between water chemistry variables to account for non-normal distributions. All statistical data analyses and visualizations were performed using R v 4.3.1 (R Development Core Team, 2023) and packages from Tidyverse (Wickham et al., 2019). All data and codes are available in a GitHub repository.

## 3. Results

### 3.1. Inter-Regional Differences in Water Chemistry Variables

Riverine Hg and DOC concentration were significantly different across all three regions with the highest median values in EI (2.5 ng Hg $L^{-1}$ and 12.5 mg C $L^{-1}$) followed by RR (1.7 ng Hg $L^{-1}$ and 5.7 mg C $L^{-1}$) and HM (1.2 ng Hg $L^{-1}$ and 6.2 mg C $L^{-1}$) (Figure 1b). The greater variance in both variables in EI could reflects the differences in their sampling designs (i.e., multi vs. single river catchments) (Figure 1b). MeHg concentrations exhibited a different inter-regional pattern, with a lower median in EI (0.08 ng $L^{-1}$) compared with HM (0.107 ng $L^{-1}$) and RR (0.109 ng $L^{-1}$). DOM fluorescence properties indicated significantly higher median terrestrial-like compounds (C1 component) and aquatically-produced compounds (C4 component) in EI (54% and 7%, respectively) than in RR (53% and 4%) and HM (50% and 4%) (Figure 1b). The inter-regional patterns in $CO_2$ and $CH_4$ concentration diverged from those of DOC. The median $CO_2$ concentration was highest in RR (0.79 mg C $L^{-1}$), followed by HM (0.53 mg C $L^{-1}$) and EI (0.40 mg C $L^{-1}$) (range: 0.11 to 3.20, Figure 1b), while the median $CH_4$ concentration was significantly higher in HM (0.01 mg C $L^{-1}$) than in RR and EI (both 0.002 mg C $L^{-1}$). The lower variance in $CO_2$ and $CH_4$ concentrations in the rivers of EI possibly reflect the dominance of larger and free-flowing rivers compared with RR and HM (Figure 1b), while the higher $CH_4$ concentration in HM could be influenced by the timing of sampling, which occurred in late summer each year.

The $\delta^{13}C$-$CO_2$ and $\delta^{13}C$-$CH_4$ varied significantly across regions, with EI showing both the highest median $\delta^{13}C$-$CO_2$ and lowest median $\delta^{13}C$-$CH_4$ (−51.1‰ and −16.9‰, respectively), corresponding to a higher $\alpha_{app}$ (1.04) (Figure 1b). This slightly higher $\alpha_{app}$ indicates less co-transformation or shared sources between the two C-gases (i.e., less exchange of lighter C isotope). More negative median $\delta^{13}C$-$CO_2$ in HM and RR (−17.6‰ and −18.4‰, respectively) could arise from more $CH_4$ oxidation or replenishment of $CO_2$ via terrestrial OM degradation along the rivers or sediments in RR and HM compared with EI. The median MOX was significantly higher in HM (0.003 mg C $L^{-1}$) than in the other two regions (0 mg C $L^{-1}$ (EI) and 0.0002 mg C $L^{-1}$ (RR)) (Figure 1b), while the median $\alpha_{app}$ varied widely across rivers (from 0.99 to 1.07 across all sites) indicating a large variability in sources and transformation processes governing $CO_2$ and $CH_4$ within each region (Figure 1).

### 3.2. Relationships Between Carbon and Mercury Forms Within and Across Regions

For nearly all correlations, considering regional patterns yielded stronger relationships compared to the overall data set fit (Figure 2a), highlighting the importance of regional properties in driving the Hg-C coupling. The Hg concentration was most strongly correlated with the DOC concentration in all three regions (*rho* = 0.57 (HM), 0.46 (RR), 0.66 (EI), Figure 2AB). The correlations between Hg concentration and DOC optical properties (incl.: C1(%) to C4(%)) were always weaker than with DOC concentrations (Figure 2AC). The direction of these correlations followed established patterns with Hg generally increasing with the dominance of the C1(%) component and decreasing with the dominance of the C4(%) component (Figure 2, Table 2 in Supporting Information S1). Correlations between the MeHg:Hg ratio and DOC concentration, C1 or C4(%) components were generally non-significant (Figure 2a).

The proportion of by-product relative to its substrate can be a good indicator of transformation processes. There was a significant positive correlation between the ratio of MeHg:Hg and the ratio of C-gases:DOC in the waters of HM and RR, except for the rivers of EI (Figures 2a and 2d). For these rivers the proportion of both MeHg and C-gases increased relative to the available pool of C and Hg substrate. The correlations between these ratios were stronger than between Hg and DOC concentrations *rho* 0.74 vs. *rho* 0.57 (HM), and *rho* 0.62 versus *rho* 0.46 (RR) (Figure 2a). In the rivers of EI, however, there was a significant positive correlation between the ratio of MeHg:Hg and the sum of $CO_2$ + $CH_4$ concentrations (*rho* 0.36, p-value 0.003) indicating a link between Hg and

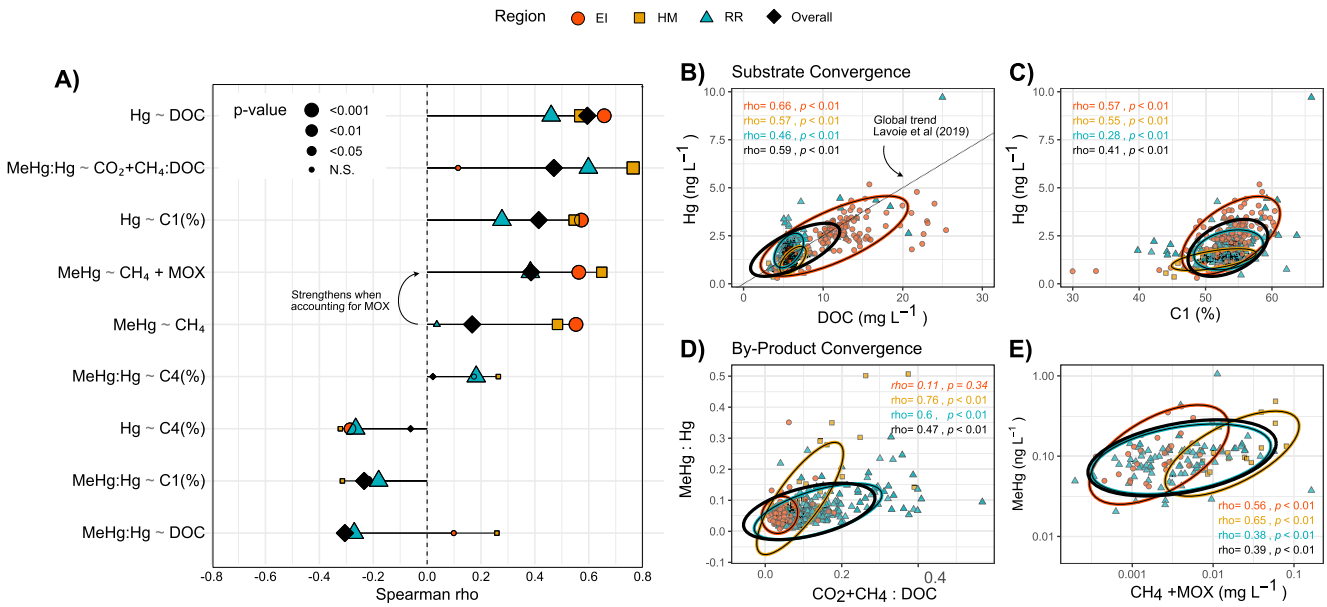


**Figure 2.** (a) Lollipop plot of the Spearman correlation coefficient (*rho*) between each pair of variables. Symbol colors and shapes denote each region (Haute-Mauricie, Romaine River, Eeyou Istchee (colored) and the overall data set (black diamonds)) for comparison. Symbol size represents the level of significance for the correlation (p-value). In (b)–(e) scatterplot of the concentrations of total dissolved mercury (Hg) against dissolved organic carbon (DOC) concentration (b) and the fraction of terrestrially derived dissolved organic matter (C1%) (c), followed by (d) the proportion of dissolved methylmercury to Hg (MeHg:Hg) as a function of the carbon gases per unit DOC ($CO_2$ + $CH_4$:DOC ratio) and (e) MeHg concentration as a function of $CH_4$ + MOX concentration, a proxy of total anaerobic C-gases concentration in mg $L^{-1}$. The ellipses in (b)–(e) mark the 95% confidence level for a multivariate t-distribution and give a visual aid of the strength and direction of the correlation for each region (colored) and for the overall data set (black). In (b), the dotted line represents the global trend (slope = 0.25) from the meta-analysis by Lavoie et al. (2019). An interactive version of the lollipop plot is available on this GitHub page.

C by-products, albeit one that is independent of the ambient DOC concentration (Figure S4 in Supporting Information S1). The correlation between the ratio of MeHg:Hg and $CO_2$ + $CH_4$ concentration was also significant in HM (*rho* 0.74, $p < 0.0001$) and RR (*rho* 0.56 $p < 0.0001$) (Figure S4 in Supporting Information S1).

MeHg concentration was positively correlated with the $CH_4$ + MOX concentration in all three regions (Figures 2a and 2e). These correlations were stronger when accounting for the combined $CH_4$ + MOX than $CH_4$ alone for rivers in HM (*rho* 0.69 vs. 0.49) and RR (*rho* 0.40 vs. 0.30), except for rivers in EI where the strength of the correlations remained similar due to overall lower MOX (*rho* 0.52 vs. 0.55) (Figure 2a). This implies that rivers where $CH_4$ concentration was higher, after accounting for both ambient and oxidized $CH_4$, were also characterized by higher MeHg concentrations.

## 4. Discussion

### 4.1. Strength of the Terrestrial Hg-DOM Coupling Across Boreal Rivers

Despite the large diversity in river characteristics in this synthesis (Figure 1), there were consistent correlations in river Hg and C concentration, speciation and properties that emerged within and among each region (Figure 2). The DOC concentration was consistently the variable most strongly correlated with Hg concentration across all three regions (Figures 2a and 2b), which agrees well with established relationships in the literature (Bravo et al., 2018; Brigham et al., 2009; Lavoie et al., 2019) (Table S2 in Supporting Information S1). The relationship between Hg and DOC concentration is typically explained by the chemical binding between Hg and OM compounds, and supports that both are predominantly co-loaded from terrestrial environments into aquatic systems (Bishop et al., 2020; Grigal, 2003; Schaefer et al., 2020). Nonetheless, the strength and direction of the relationship between river Hg and DOC concentration were noticeably variable across individual regions, suggesting region-specific drivers in the transport and transformation of the Hg-OM complex (Figure 2b; *rho* 0.46 to 0.66) (Lavoie et al., 2019).

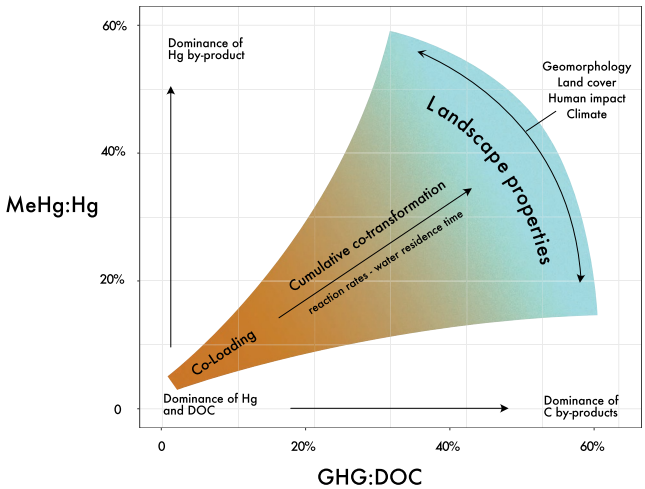


**Figure 3.** Conceptual scheme of the local riverine and landscape properties that could influence the co-transformation of Hg and dissolved organic carbon within rivers based on this study and the findings of (Bonville et al., 2020; Fink-Mercier, Giorgio, et al., 2022; Ponton et al., 2021).

A growing number of studies have reported that terrestrial indices of DOM composition, such as DOM with higher aromaticity (Burns et al., 2012; Dittman et al., 2009), abundance of humic acids (Bravo et al., 2017; Haitzer et al., 2002), or higher molecular weight or DOC age (e.g., Campeau et al., 2022; Lescord et al., 2018), can surpass DOC concentration as predictors of Hg concentration in surface water (Table S2 in Supporting Information S1). The positive correlation between Hg and the terrestrially-derived C1 component across rivers of all regions supports that Hg is more closely associated with the terrestrially-derived portion of DOM (Bishop et al., 2020; Haitzer et al., 2002) than aquatic-derived or freshly produced DOM (C4) (Bravo et al., 2017) (Figures 2a–2c). However, the weakness of this correlation suggests that processes other than co-loading also affect the Hg-DOM complex along its transport in these rivers. These additional processes could involve transport or transformation processes (Garcia et al., 2005; O'Driscoll et al., 2006) and contribute to blurring the relationship between Hg and terrestrial DOM, all of which may be influenced by landscape properties that vary across these three regions.

### 4.2. Co-Transformation of the Hg-DOM Complex in Rivers

General associations between river MeHg and C-gases concentrations have emerged from individual river catchment studies (Amyot et al., 2024; Bonville et al., 2020; MacMillan et al., 2015). Our synthesis corroborates these findings across three separate regions by providing two separate pieces of evidence for this general association. First, the positive correlation between the proportion MeHg per unit Hg and of C-gases per unit DOC (Figure 2d), suggests proportional transformation rates of the Hg and DOC within these rivers. Secondly, the correlation between MeHg and total $CH_4$ concentration, comprising both the ambient and oxidized fractions reconstructed from isotopic proxies (Figure 2e), provides mechanistic evidence for this co-transformation of Hg and C in these rivers or their connecting surrounding habitats. Since production of MeHg and $CH_4$ in rivers occurs mostly by microbes in hyporheic sediments (Nasr & Arp, 2017; Pak & Bartha, 1998), it allows for a potentially large fraction of the $CH_4$ to be oxidized by the time it reaches the water's surface (Shelley et al., 2017). The influence of $CH_4$ oxidation was most evident in the waters of RR and HM, where it masked an underlying link between MeHg and $CH_4$ (Figure 2a), an effect that can be partially retro-calculated using $\delta^{13}$C-values.

This synthesis also highlights intriguing differences in the strength and directionality of the correlations between various Hg and C forms across the three studied regions (Figure 2). The sampling design for each region, focusing on a single river continuum (RR and HM) or multiple river systems (EI), and incorporating various seasons and degrees of river harnessing, could influence our interpretation of these inter-regional differences (Bonville et al., 2020; Fink-Mercier, Giorgio, et al., 2022; Ponton et al., 2021). However, intrinsic landscape properties could also influence the coupling between various Hg and C forms by shifting the influence of co-loading, co-transport and co-transformation (Figure 3). In the rivers of EI, which is the coldest and most wetland-dominated region of the three (Figure 1a), the correlation between Hg and DOC substrate forms emerged as the predominant relationships (Figure 2a), indicating that co-loading could be the main process underlying the cycling of Hg and C in these rivers (bottom-left corner of Figure 3) (Burns et al., 2012; Campeau et al., 2022; Fink-Mercier, Giorgio, et al., 2022).

This terrestrial co-loading signal can be gradually replaced by co-transformation within rivers when water residence time or reaction rates increase (Branfireun et al., 2020; Catalán et al., 2016; Richardson et al., 2020) (slope of Figure 3). These processes are largely influenced by river hydrology, which itself responds to multiple landscape properties, such as geomorphology (e.g., channel morphology, slope), land cover (e.g., wetland and forest cover), human impact (e.g., impoundments and flow regulation), and climate (temperature, precipitation and surface runoff). The shift toward more co-transformation was most evident in the waters of HM, which is the warmest region of the three, and in RR, which is the most recently impounded river (Amyot et al., 2024; Millera Ferriz et al., 2021; Ponton et al., 2021). Distinct landscape properties may disproportionally stimulate the cycling of Hg versus C (shifting slope on Figure 3), potentially leading them to decouple over time due to different turnover and loss rates of MeHg and C-gases in river systems. While we cannot resolve which landscape

properties drive these shifting correlations, our findings emphasize a persistent interconnection in the biogeochemical cycling of Hg and C forms, despite their distinct transformation pathways.

In conclusion, this synthesis demonstrates an apparent convergence in the patterns of loading, transport and transformation of Hg and C across many boreal rivers. However, these relationships are not uniformly expressed across the landscape, which indicates that regional landscape properties may modulate these processes. The by-products that arise from the co-transformation of Hg and DOM have environmental relevance with respect to freshwater quality, community health, and global warming. Larger field surveys, with a more replicable sampling design, will be essential to better identify these landscape drivers and how they may respond to direct or indirect disturbances that continue to modify watershed processes. Nonetheless, our results suggest that landscape properties known to increase one of these Hg and C forms may lead to increases in the other, and conversely, therefore emphasizing the intricate coupling between Hg and C biogeochemical cycling.

## Data Availability Statement

The data set for this manuscript is available at Campeau (2025).

**Acknowledgments**
This study was supported by an NSERC-CRD Grant to M.A., J.F.L. and P.D.G. in partnership with Hydro-Québec. This work has benefited from the support of the Groupe de Recherche Interuniversitaire en Limnologie (GRIL), supported by Fonds de Recherche du Québec, secteur Nature et Technologies. Niskamoon Corporation. Canadian Foundation for Innovation. Special thanks to Dominic Bélanger in the lab and numerous field assistants. Additional support from FORMAS, the Swedish Research Council for Sustainable Development to A.C. (Grant 2019-01592) is also acknowledged. We acknowledge the presence and contribution of the Innu (RR), Atikamekw (HM) and Cree (EI) communities in the studied regions.

## References

Amyot, M., Bilodeau, F., Tremblay, A., Planas, D., Walsh, D., & Ponton, D. E. (2024). Cumulative effects of watershed disturbances and run-of-river dams on mercury cycling: Case study and recommendations for environmental managers. *Environmental Management*. https://doi.org/10.1007/s00267-024-01990-6

Bishop, K., Shanley, J. B., Riscassi, A., de Wit, H. A., Eklof, K., Meng, B., et al. (2020). Recent advances in understanding and measurement of mercury in the environment: Terrestrial Hg cycling. *Science of the Total Environment*, *721*, 137647. https://doi.org/10.1016/j.scitotenv.2020.137647

Branfireun, B. A., Cosio, C., Poulain, A. J., Riise, G., & Bravo, A. G. (2020). Mercury cycling in freshwater systems–An updated conceptual model. *Science of the Total Environment*, *745*, 140906. https://doi.org/10.1016/j.scitotenv.2020.140906

Braune, B., Chetelat, J., Amyot, M., Brown, T., Clayden, M., Evans, M., et al. (2015). Mercury in the marine environment of the Canadian Arctic: Review of recent findings. *Science of the Total Environment*, *509–510*, 67–90. https://doi.org/10.1016/j.scitotenv.2014.05.133

Bravo, A. G., Bouchet, S., Tolu, J., Bjorn, E., Mateos-Rivera, A., & Bertilsson, S. (2017). Molecular composition of organic matter controls methylmercury formation in boreal lakes. *Nature Communications*, *8*(1), 14255. https://doi.org/10.1038/ncomms14255

Bravo, A. G., Kothawala, D. N., Attermeyer, K., Tessier, E., Bodmer, P., Ledesma, J. L. J., et al. (2018). The interplay between total mercury, methylmercury and dissolved organic matter in fluvial systems: A latitudinal study across Europe. *Water Research*, *144*, 172–182. https://doi.org/10.1016/j.watres.2018.06.064

Brigham, M. E., Wentz, D. A., Aiken, G. R., & Krabbenhoft, D. P. (2009). Mercury cycling in stream ecosystems. 1. Water column chemistry and transport. *Environmental Science & Technology*, *43*(8), 2720–2725. https://doi.org/10.1021/es802694n

Burns, D. A., Aiken, G. R., Bradley, P. M., Journey, C. A., & Schelker, J. (2012). Specific ultra-violet absorbance as an indicator of mercury sources in an Adirondack River basin. *Biogeochemistry*, *113*(1–3), 451–466. https://doi.org/10.1007/s10533-012-9773-5

Campeau, A. (2025). Dataset for Coupling between methylmercury and carbon-gases across boreal rivers of Québec, Canada, (Version 1.0) [Dataset]. *Borealis*. https://doi.org/10.5683/SP3/FCMJYR

Campeau, A., Eklof, K., Soerensen, A. L., Akerblom, S., Yuan, S., Hintelmann, H., et al. (2022). Sources of riverine mercury across the Mackenzie River Basin; inferences from a combined HgC isotopes and optical properties approach. *Science of the Total Environment*, *806*(Pt 4), 150808. https://doi.org/10.1016/j.scitotenv.2021.150808

Campeau, A., Lapierre, J. F., Vachon, D., & del Giorgio, P. A. (2014). Regional contribution of $CO_2$ and $CH_4$ fluxes from the fluvial network in a lowland boreal landscape of Quebec. *Global Biogeochemical Cycles*, *28*(1), 57–69. https://doi.org/10.1002/2013GB004685

Campeau, A., Wallin, M. B., Giesler, R., Lofgren, S., Morth, C. M., Schiff, S., et al. (2017). Multiple sources and sinks of dissolved inorganic carbon across Swedish streams, refocusing the lens of stable C isotopes. *Scientific Reports*, *7*(1), 9158. https://doi.org/10.1038/s41598-017-09049-9

Catalán, N., Marcé, R., Kothawala, D. N., & Tranvik, L. J. (2016). Organic carbon decomposition rates controlled by water retention time across inland waters. *Nature Geoscience*, *9*(7), 501–504. https://doi.org/10.1038/ngeo2720

De Bonville, J., Amyot, M., del Giorgio, P., Tremblay, A., Bilodeau, F., Ponton, D. E., & Lapierre, J. F. (2020). Mobilization and transformation of mercury across a dammed boreal river are linked to carbon processing and hydrology. *Water Resources Research*, *56*(10), e2020WR027951. https://doi.org/10.1029/2020wr027951

Dittman, J. A., Shanley, J. B., Driscoll, C. T., Aiken, G. R., Chalmers, A. T., & Towse, J. E. (2009). Ultraviolet absorbance as a proxy for total dissolved mercury in streams. *Environmental Pollution*, *157*(6), 1953–1956. https://doi.org/10.1016/j.envpol.2009.01.031

Driscoll, C. T., Mason, R. P., Chan, H. M., Jacob, D. J., & Pirrone, N. (2013). Mercury as a global pollutant: Sources, pathways, and effects. *Environmental Science & Technology*, *47*(10), 4967–4983. https://doi.org/10.1021/es305071v

Emmerton, C. A., Drevnick, P. E., Serbu, J. A., Cooke, C. A., Graydon, J. A., Reichert, M., et al. (2022). Downstream modification of mercury in diverse river systems underscores the role of local conditions in fish bioaccumulation. *Ecosystems*, *26*(1), 114–133. https://doi.org/10.1007/s10021-022-00745-w

Fink-Mercier, C., del Giorgio, P. A., Amyot, M., & Lapierre, J. F. (2022a). Hydrology and seasonality shape the coupling of dissolved Hg and methyl-Hg with DOC in boreal rivers in northern Québec. *Water Resources Research*, *58*(12), e2022WR033036. https://doi.org/10.1029/2022WR033036

Fink Mercier, C., Lapierre, J. F., Amyot, M., & del Giorgio, P. A. (2022b). Concentrations and yields of total Hg and MeHg in large boreal rivers linked to water and wetland coverage in the watersheds. *Journal of Geophysical Research: Biogeosciences*, *127*(5), e2022JG006892. https://doi.org/10.1029/2022jg006892

Garcia, E., Amyot, M., & Ariya, P. A. (2005). Relationship between DOC photochemistry and mercury redox transformations in temperate lakes and wetlands. *Geochimica et Cosmochimica Acta*, *69*(8), 1917–1924. https://doi.org/10.1016/j.gca.2004.10.026

Grigal, D. F. (2003). Mercury sequestration in forests and peatlands: A review. *Journal of Environmental Quality*, *32*(2), 393–405. https://doi.org/10.2134/jeq2003.0393

Haitzer, M., Aiken, G. R., & Ryan, J. N. (2002). Binding of Mercury(II) to dissolved organic matter: The role of the mercury-to-DOM concentration ratio. *Environmental Science & Technology*, *36*(16), 3564–3570. https://doi.org/10.1021/es025699i

Hebert, C. E. (2019). The river runs through it: The Athabasca River delivers mercury to aquatic birds breeding far downstream. *PLoS One*, *14*(4), e0206192. https://doi.org/10.1371/journal.pone.0206192

Kothawala, D. N., Stedmon, C. A., Muller, R. A., Weyhenmeyer, G. A., Kohler, S. J., & Tranvik, L. J. (2014). Controls of dissolved organic matter quality: Evidence from a large-scale boreal lake survey. *Global Change Biology*, *20*(4), 1101–1114. https://doi.org/10.1111/gcb.12488

Lapierre, J. F., & del Giorgio, P. A. (2014). Partial coupling and differential regulation of biologically and photochemically labile dissolved organic carbon across boreal aquatic networks. *Biogeosciences*, *11*(20), 5969–5985. https://doi.org/10.5194/bg-11-5969-2014

Lavoie, R. A., Amyot, M., & Lapierre, J. F. (2019). Global meta-analysis on the relationship between mercury and dissolved organic carbon in freshwater environments. *Journal of Geophysical Research: Biogeosciences*, *124*(6), 1508–1523. https://doi.org/10.1029/2018jg004896

Lawruk-Desjardins, C., Storck, V., Ponton, D. E., Amyot, M., & Walsh, D. A. (2024). A genome catalogue of mercury-methylating bacteria and archaea from sediments of a boreal river facing human disturbances. *Environmental Microbiology*, *26*(6), e16669. https://doi.org/10.1111/1462-2920.16669

Lescord, G. L., Emilson, E. J. S., Johnston, T. A., Branfireun, B. A., & Gunn, J. M. (2018). Optical properties of dissolved organic matter and their relation to mercury concentrations in water and biota across a remote freshwater drainage basin. *Environmental Science & Technology*, *52*(6), 3344–3353. https://doi.org/10.1021/acs.est.7b05348

MacMillan, G. A., Girard, C., Chételat, J., Laurion, I., & Amyot, M. (2015). High methylmercury in arctic and subarctic ponds is related to nutrient levels in the warming eastern Canadian arctic. *Environmental Science & Technology*, *49*(13), 7743–7753. https://doi.org/10.1021/acs.est.5b00763

Millera Ferriz, L., Ponton, D. E., Storck, V., Leclerc, M., Bilodeau, F., Walsh, D. A., & Amyot, M. (2021). Role of organic matter and microbial communities in mercury retention and methylation in sediments near run-of-river hydroelectric dams. *Science of the Total Environment*, *774*, 145686. https://doi.org/10.1016/j.scitotenv.2021.145686

Nasr, M., & Arp, P. A. (2017). Mercury and organic matter concentrations in lake and stream sediments in relation to one another and to atmospheric mercury deposition and climate variations across Canada. *Journal of Chemistry*, *2017*, 1–21. https://doi.org/10.1155/2017/8949502

O'Driscoll, N. J., Siciliano, S. D., Lean, D. R., & Amyot, M. (2006). Gross photoreduction kinetics of mercury in temperate freshwater lakes and rivers: Application to a general model of DGM dynamics. *Environmental Science & Technology*, *40*(3), 837–843. https://doi.org/10.1021/es051062y

Pak, K. R., & Bartha, R. (1998). Mercury methylation and demethylation in anoxic lake sediments and by strictly anaerobic bacteria. *Applied and Environmental Microbiology*, *64*(3), 1013–1017. https://doi.org/10.1128/aem.64.3.1013-1017.1998

Ponton, D. E., Lavoie, R. A., Leclerc, M., Bilodeau, F., Planas, D., & Amyot, M. (2021). Understanding food web mercury accumulation through trophic transfer and carbon processing along a river affected by recent run-of-river dams. *Environmental Science & Technology*, *55*(5), 2949–2959. https://doi.org/10.1021/acs.est.0c07015

Raymond, P. A., Hartmann, J., Lauerwald, R., Sobek, S., McDonald, C., Hoover, M., et al. (2013). Global carbon dioxide emissions from inland waters. *Nature*, *503*(7476), 355–359. https://doi.org/10.1038/nature12760

Richardson, M., Chételat, J., MacMillan, G. A., & Amyot, M. (2020). Mercury concentrations and associations with dissolved organic matter are modified by water residence time in eastern Canadian lakes along a 30° latitudinal gradient. *Limnology & Oceanography*, *66*(S1). https://doi.org/10.1002/lno.11580

Rocher-Ros, G., Stanley, E. H., Loken, L. C., Casson, N. J., Raymond, P. A., Liu, S., et al. (2023). Global methane emissions from rivers and streams. *Nature*, *621*(7979), 530–535. https://doi.org/10.1038/s41586-023-06344-6

Schaefer, K., Elshorbany, Y., Jafarov, E., Schuster, P. F., Striegl, R. G., Wickland, K. P., & Sunderland, E. M. (2020). Potential impacts of mercury released from thawing permafrost. *Nature Communications*, *11*(1), 4650. https://doi.org/10.1038/s41467-020-18398-5

Schartup, A. T., Balcom, P. H., Soerensen, A. L., Gosnell, K. J., Calder, R. S., Mason, R. P., & Sunderland, E. M. (2015). Freshwater discharges drive high levels of methylmercury in Arctic marine biota. *Proceedings of the National Academy of Sciences of the U S A*, *112*(38), 11789–11794. https://doi.org/10.1073/pnas.1505541112

Selin, N. E. (2009). Global biogeochemical cycling of mercury: A review. *Annual Review of Environment and Resources*, *34*(1), 43–63. https://doi.org/10.1146/annurev.environ.051308.084314

Shelley, F., Ings, N., Hildrew, A. G., Trimmer, M., & Grey, J. (2017). Bringing methanotrophy in rivers out of the shadows. *Limnology & Oceanography*, *62*(6), 2345–2359. https://doi.org/10.1002/lno.10569

Skyllberg, U., Bloom, P. R., Qian, J., Lin, C. M., & Bleam, W. F. (2006). Complexation of Mercury(II) in soil organic matter: EXAFS evidence for linear two-coordination with reduced sulfur groups. *Environmental Science & Technology*, *40*(13), 4174–4180. https://doi.org/10.1021/es0600577

Tarnocai, C., Kettles, & Lacette. (2011). Peatlands of Canada.

Thottathil, S. D., Reis, P. C. J., del Giorgio, P. A., & Prairie, Y. T. (2018). The extent and regulation of summer methane oxidation in northern lakes. *Journal of Geophysical Research: Biogeosciences*, *123*(10), 3216–3230. https://doi.org/10.1029/2018JG004464

Ullrich, S. M., Tanton, T. W., & Abdrashitova, S. A. (2001). Mercury in the aquatic environment: A review of factors affecting methylation. *Critical Reviews in Environmental Science and Technology*, *31*(3), 241–293. https://doi.org/10.1080/20016491089226

Whiticar, M. J. (1999). Carbon and hydrogen isotope systematics of bacterial formation and oxidation of methane. *Chemical Geology*, *161*(1–3), 291–314. https://doi.org/10.1016/S0009-2541(99)00092-3

Wickham, H., Averick, M., Bryan, J., Chang, W., McGowan, L., François, R., et al. (2019). Welcome to the Tidyverse. *Journal of Open Source Software*, *4*(43), 1686. https://doi.org/10.21105/joss.01686

Zhu, W., Song, Y., Adediran, G. A., Jiang, T., Reis, A. T., Pereira, E., et al. (2018). Mercury transformations in resuspended contaminated sediment controlled by redox conditions, chemical speciation and sources of organic matter. *Geochimica et Cosmochimica Acta*, *220*, 158–179. https://doi.org/10.1016/j.gca.2017.09.045

## References From the Supporting Information

Jutaporn, P., Armstrong, M. D., & Coronell, O. (2020). Assessment of C-DBP and N-DBP formation potential and its reduction by MIEX® DOC and MIEX® GOLD resins using fluorescence spectroscopy and parallel factor analysis. *Water Research*, *172*, 115460. https://doi.org/10.1016/j.watres.2019.115460

Murphy, K. R., Hambly, A., Singh, S., Henderson, R. K., Baker, A., Stuetz, R., & Khan, S. J. (2011). Organic matter fluorescence in municipal water recycling schemes: Toward a unified PARAFAC model. *Environmental Science & Technology*, *45*(7), 2909–2916. https://doi.org/10.1021/es103015e

Osburn, C. L., Anderson, N. J., Stedmon, C. A., Giles, M. E., Whiteford, E. J., McGenity, T. J., et al. (2017). Shifts in the source and composition of dissolved organic matter in Southwest Greenland lakes along a regional hydro-climatic gradient. *Journal of Geophysical Research: Biogeography*, *122*(12), 3431–3445. https://doi.org/10.1002/2017jg003999

Osburn, C. L., Boyd, T. J., Montgomery, M. T., Bianchi, T. S., Coffin, R. B., & Paerl, H. W. (2016). Optical proxies for terrestrial dissolved organic matter in estuaries and coastal waters. *Frontiers in Marine Science*, *2*, 127. https://doi.org/10.3389/fmars.2015.00127

Shutova, Y., Baker, A., Bridgeman, J., & Henderson, R. K. (2014). Spectroscopic characterisation of dissolved organic matter changes in drinking water treatment: From PARAFAC analysis to online monitoring wavelengths. *Water Research*, *54*, 159–169. https://doi.org/10.1016/j.watres.2014.01.053

Stedmon, C. A., & Markager, S. (2005). Resolving the variability in dissolved organic matter fluorescence in a temperate estuary and its catchment using PARAFAC analysis. *Limnology & Oceanography*, *50*(2), 686–697. https://doi.org/10.4319/lo.2005.50.2.0686